A Closed-Loop Phase-Locked Interferometer for Wide Bandwidth Position Sensing

Andrew J. Fleming[1, a)] and Ben S. Routley[1, b)]
School of Electrical Engineering and Computer Science, University of Newcastle, Callaghan, NSW 2308, Australia.

(Dated: 27 October 2015)

This article describes a position sensitive interferometer with closed-loop control of the reference mirror. A calibrated nanopositioner is used to lock the interferometer phase to the most sensitive point in the interferogram. In this configuration, large low-frequency movements of the sensor mirror can be detected from the control signal applied to the nanopositioner and high-frequency short-range signals can be measured directly from the photodiode. It is demonstrated that these two signals are complementary and can be summed to find the total displacement. The resulting interferometer has a number of desirable characteristics: it is optically simple, does not require polarization or modulation to detect the direction of motion, does not require fringe-counting or interpolation electronics, and has a bandwidth equal to that of the photodiode. Experimental results demonstrate the frequency response analysis of a high-speed positioning stage. The proposed instrument is ideal for measuring the frequency response of nanopositioners, electro-optical components, MEMs devices, Ultrasonic devices, and sensors such as surface acoustic wave detectors.

I. INTRODUCTION

The sensing requirements in precision mechatronic systems are among the most demanding of any control application[1]. The sensors must be compact, high-speed, immune to environmental variation, and able to resolve position down to the atomic scale[2].

To achieve high absolute accuracy over a large range, the reference standard is the laser heterodyne interferometer[3]. Since 1960, the meter length standard has been defined by optical means. This change arose after Michelson invented the interferometer which improved the accuracy of length measurement[4] from a few parts in 10^7, to a few parts in 10^9. Thus, in 1960, the meter was redefined in terms of the orange line from a ^{86}Kr discharge lamp. Although bulky and costly, the interferometer has been the sensor of choice for applications such as IC wafer steppers[5,6] and metrological systems[7].

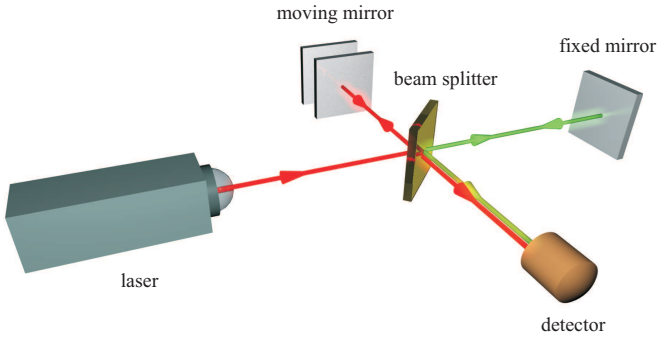

FIG. 1. The operation of a displacement sensitive Michelson interferometer. The laser light is split into two paths, one that is reflected by a target mirror and another that is reflected from a reference mirror. The two beams are recombined and interfere at the detector. If the path length difference is an integer number of half-wavelengths, constructive interference occurs.

The operating principle of a Michelson interferometer is described in Figure 1. A laser beam is split into two paths, one that is reflected by a target mirror and another that is reflected by a reference mirror. The movement of the mirror is measurable by observing the intensity at the detector. If the path length difference is an integer number of half-wavelengths, constructive interference occurs. The displacement of the moving mirror, in half-wavelengths, is measured by counting the number of intensity peaks at the photodiode. The phase of the interference, and hence the displacement between intensity peaks, can also be derived from the detector intensity.

Although simple, the Michelson interferometer is rarely used directly for displacement metrology since the sensitivity is a function of the path length and there is no directional information. Modern displacement interferometers are based on the Heterodyne interferometer by Duke and Gordon from Hewlett-Packard in 1970[8]. Although similar in principle to a Michelson interferometer, the heterodyne interferometer, overcomes many of the problems associated with the Michelson design. Most importantly, the phase sensitivity remains constant regardless of the path length difference.

Since the original work in 1970, a wide variety of improvements have been made to the basic heterodyne interferometer[9]. All of these devices work on the heterodyne principle, where the displacement is proportional to the phase (or frequency) difference between two laser beams. In heterodyne interferometers, the displacement signal is modulated to avoid $1/f$ noise and low-frequency light-source intensity variations. Other advances include the low-finesse Fabry-Perot interferometer[10], which has a small fiber-coupled measurement head.

a) Andrew.Fleming@Newcastle.edu.au
b) Ben.Routley@Newcastle.edu.au

A drawback of conventional interferometers is the cost, optical complexity, and large physical size. The bandwidth is also limited by the speed of fringe-counting and interpolation electronics. For these reasons, capacitive sensors or similar are more often used for measuring the response of high-speed mechatronic systems. Although simple, these sensors are limited in bandwidth to approximately 100 kHz and must be mounted in close proximity to the moving object. To overcome the limitations of such sensors, a need exists for a simple, low-cost interferometer that is suitable for remote measurement of high-frequency motion.

To achieve a wide measurement bandwidth, a number of articles have reported methods for tuning the path length difference of a Michelson interferometer to $(n + \lambda/4)$. At this operating point, the photodiode intensity is approximately proportional to small changes in the path length difference due to the small angle approximation, i.e. when $\sin\theta \approx \theta$. The path length difference can be fixed at this operating point by applying a correction voltage to a piezoelectric actuated reference mirror[11,12]. In these examples, laser generated acoustic waves were measured for material analysis, yielding a sensitivity of approximately 0.02 nm and a bandwidth of 30 MHz[13].

In this work, a refinement of historical methods is described which yields similarly wide bandwidth but a travel range on the order of 100 μm or more. In the following section, a Michelson interferometer is described with closed-loop control of the reference mirror. In Sections III and IV, it is demonstrated that large low-frequency movements of the sensor mirror can be detected from the control signal applied to the nanopositioner and high-frequency short-range signals can be measured directly from the photodiode signal. These two signals are shown to be mathematically complementary so they can be summed to find the total displacement.

The resulting interferometer has a number of desirable characteristics, it is optically simple, does not require polarization or modulation to detect the direction of motion, does not require fringe-counting or interpolation electronics, and has a bandwidth equal to that of the photodiode. Experimental results in Section VII demonstrate the frequency response analysis of a high-speed positioning stage. The proposed instrument is ideal for measuring the frequency response of devices such as nanopositioners[14,15]and microcantilevers[16]. Other measurement applications include electro-optics, MEMs devices, Ultrasonic devices, and sensors such as surface acoustic wave detectors.

II. INTERFEROMETER DESIGN

The optical design is identical to a basic Michelson Interferometer except that the reference mirror is mounted on a nanopositioning stage. As illustrated in Figure 2, collimated light from a Helium-Neon laser with a wavelength of 632.8 nm is passed through a 50/50 non-polarizing beam splitter forming two beam paths. One beam is reflected off the sensor mirror and then superimposed with the other beam which has been reflected off the reference mirror. The reference mirror is mounted on a Queensgate NPS-X-15D single-axis nanopositioner. The superimposed beam is then passed through a 20X objective lens to expand the beam. This expanded beam is directed to a high bandwidth apertured silicon photodetector. The amplified signal produced by the photodetector will is a sinusoidal function of the path length difference, that is

$$I = \frac{1}{2} I_0 \left(1 + \cos\left(\frac{4\pi}{\lambda} \left(d_r - d_s \right) \right) \right), \tag{1}$$

where I is the intensity, I_0 is the maximum intensity, and λ is the laser wavelength. For simplicity in the control-loop it is beneficial to normalize the photodiode signal to ± 1, which involves subtracting $I_0/2$ and scaling by $2/I_0$. After this adjustment, the photodiode signal becomes

$$p = \cos\left(\frac{4\pi}{\lambda} \left(d_r - d_s \right) \right). \tag{2}$$

This function is plotted in Figure 3 together with the operating point of the interferometer. Note that for small deviations around the angle $3\pi/2$, the response is a linear function of displacement.

The experimental setup corresponding to the diagram in Figure 2 is pictured in Figure 4. The device under test is mounted in the upper left quadrant of the photograph. The small number of optical components illustrates the simplicity of the proposed design.

One undesirable practical characteristic of the Michelson arrangement is that light is returned to the laser when the photodiode intensity is at a null. This can be avoided by optical means using polarization or a Faraday Isolator; however, a simpler solution is to offset the mirror

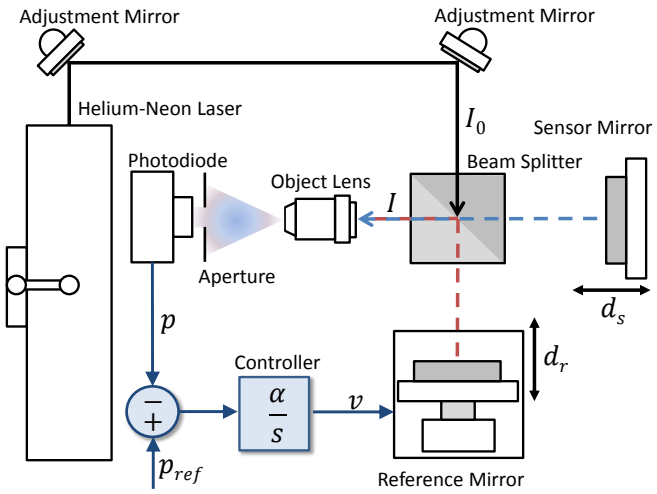

FIG. 2. Schematic of the optical arrangement

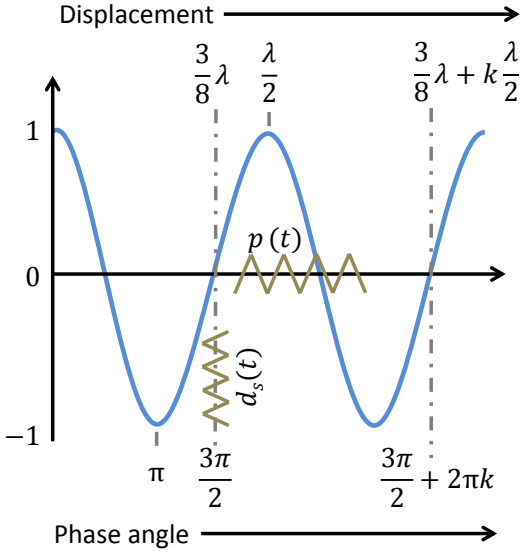

FIG. 3. The scaled photodiode signal p versus the phase angle and displacement.

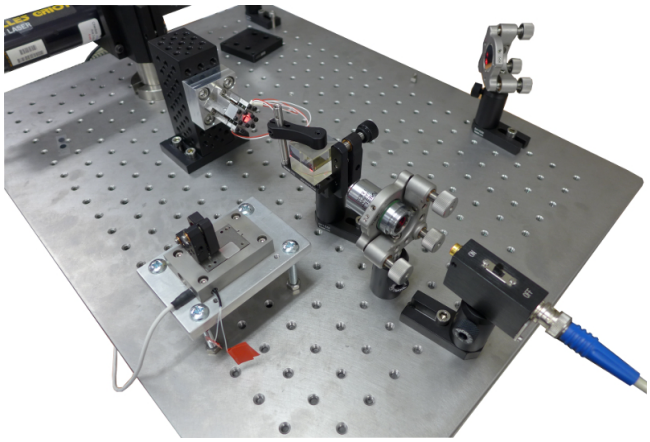

FIG. 4. The experimental setup showing the device under test (upper left) and the interferometer optical path.

angle slightly so that the returned beam does not enter the laser aperture. Although this approach eliminates laser feedback, the alignment becomes a function of the mirror displacement which is undesirable. However due to the small maximum displacement changes relative to the path lengths used 10 um vs 150 mm, this effect is negligible.

III. INTERFEROMETER MODELING

The signal block diagram of the proposed interferometer is illustrated in Figure 5. An integral controller is chosen so that the closed-loop response will be approximately first-order.

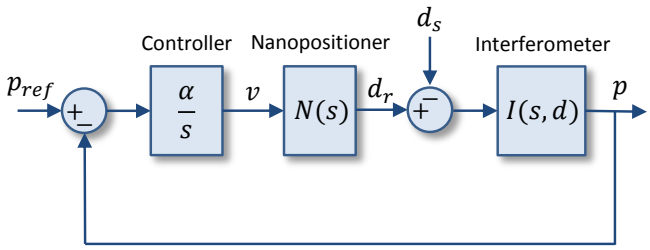

FIG. 5. Block diagram of the closed-loop interferometer. The set-point for the scaled photodiode signal is $p_{ref} = 0$, which drives the reference mirror position d_r so that the interferometer phase is locked to $3\pi/2$. The position d_s of the sensing mirror enters the system as disturbance and is suppressed by the control system. At steady-state, the controller acts to ensure that $d_r = d_s$.

The nanopositioner $N(s)$ is commanded by a voltage v and develops a displacement d_r of the reference mirror. Assuming that the resonance frequency of the positioning stage is much higher than the control-loop bandwidth, the response can be approximated by a constant gain of k_n μm/V. That is, the nanopositioner response is assumed to be

$$N(s) = k_n. \tag{3}$$

As described in the previous section, the interferometer is sensitive to the path length difference between the reference and sensing mirrors. Assuming that the interferogram signal from the photodiode is scaled to ± 1, the interferometer model is

$$I(s,d) = \frac{p(s)}{d_r(s) - d_s(s)} = \cos\left(\frac{4\pi}{\lambda}\left(d_r - d_s\right)\right) \tag{4}$$

If the photodiode signal is maintained at $p = 0$, the above model has stable operating points when the phase is

$$\theta = \frac{6\pi}{4} + k2\pi \quad k \in \mathcal{I}, \tag{5}$$

which is equivalent to

$$(d_r - d_s) = \frac{3}{8}\lambda + k\frac{\lambda}{2} \quad k \in \mathcal{I}. \tag{6}$$

At these operating points, the small signal response is linear with a sensitivity of $4\pi/\lambda$. Therefore, for small signals, the interferometer model is

$$I(s) = \frac{4\pi}{\lambda}. \tag{7}$$

IV. INTERFEROMETER CONTROL AND DETECTION

Based on the diagram in Figure 5, the complementary sensitivity function is

$$\frac{p(s)}{p_{ref}(s)} = \frac{\frac{\alpha}{s}N(s)I(s)}{1 + \frac{\alpha}{s}N(s)I(s)}, \tag{8}$$

which is equal to

$$\frac{p(s)}{p_{ref}(s)} = \frac{\alpha k_n 4\pi/\lambda}{s + \alpha k_n 4\pi/\lambda}. \tag{9}$$

This response is a unity-gain first-order low-pass filter with a cut-off frequency of $\omega_c = \alpha k_n 4\pi/\lambda$ rad/s.

The position of the sensing mirror enters the feedback loop as a disturbance. The transfer function from the sensing mirror position d_s to the control signal v is

$$\frac{v(s)}{d_s(s)} = \frac{-\alpha 4\pi/\lambda}{s + \alpha k_n 4\pi/\lambda}. \tag{10}$$

Which is a first-order low-pass filter with a gain of $-1/k_n$. That is, at frequencies below ω_c, the position of the sensing mirror is proportional to the control signal v with a sensitivity of $-1/k_n$ V/μm.

Using a similar procedure, the transfer function from the sensing mirror position d_s to the photodiode signal p is

$$\frac{p(s)}{d_s(s)} = \frac{4\pi/\lambda s}{s + \alpha k_n 4\pi/\lambda}. \tag{11}$$

Which is a first-order high-pass filter with a gain of $4\pi/\lambda$. That is, at frequencies above ω_c, the position of the sensing mirror is proportional to the photodiode signal p with a sensitivity of $4\pi/\lambda$ V/m.

It can be observed that when the transfer functions (10) and (11) are scaled to the same units, they are complementary, that is, they sum to unity. This implies the that the position of the sensing mirror can be completely recovered by adding together scaled versions of the control signal v and photodiode signal p. Consider the sum,

$$\widehat{d_s}(s) = -k_n v(s) + \frac{\lambda}{4\pi} p(s). \tag{12}$$

By substituting (10) and (11)

$$\frac{\widehat{d_s}}{d_s(s)} = -k_n \frac{-\alpha 4\pi/\lambda}{s + \alpha k_n 4\pi/\lambda} + \frac{\lambda}{4\pi} \frac{4\pi/\lambda s}{s + \alpha k_n 4\pi/\lambda}. \tag{13}$$

$$\frac{\widehat{d_s}}{d_s(s)} = \frac{s + \alpha k_n 4\pi/\lambda}{s + \alpha k_n 4\pi/\lambda} = 1. \tag{14}$$

Therefore, the sum in (12) recovers the position of the sensing mirror. This arrangement is illustrated in Figure 6. The controller command signal is the only signal in the feedback loop which is complementary to the photodiode signal.

V. INTERFEROMETER CHARACTERISTICS

The proposed interferometer has a number of beneficial characteristics. Firstly, the optical arrangement is the simplest possible of any interferometer. The optical path is identical to the most simple type of Michelson interferometer. There is no polarization, $\lambda/4$ wave plates, or modulation required to detect the direction of motion. Furthermore, there is no requirement for fringe-counting or interpolation electronics and the interferometer is always operating at the most sensitive phase. The second major benefit is the bandwidth; since there is no demodulation or interpolation required, the bandwidth is only limited to that of the photodiode, which can be in the hundreds of MHz. Therefore, the proposed interferometer is ideal for direct vibration measurement of high frequency MEMs devices, electroactive crystals, and devices such as Surface Acoustic Wave (SAW) detectors.

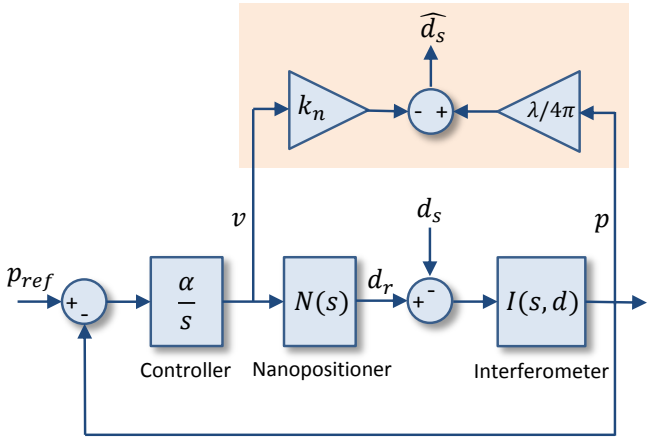

FIG. 6. Block diagram of the closed-loop interferometer with estimation of the sensing mirror displacement.

The foremost disadvantage of the proposed design is that the range is limited by the nanopositioner. Therefore, the applications are limited to those with small displacement ranges. Secondly, at frequencies above ω_c the linearity and range is determined by the cosine function of the interferogram which has a period of $\lambda/2$. To maintain a phase variation of less than $2\pi/10$, the maximum peak-to-peak high-frequency amplitude is $\lambda/20$. To avoid a jump in the operating point, the maximum high-frequency phase variation is $\pm\pi/2$, which is equivalent to a maximum displacement of $\pm\lambda/8$.

A number of design improvements are possible. To improve the stability of the interferogram, the laser output could be sampled to normalize the photodiode signal with respect to the laser power. This would also reduce or eliminate sensing noise due to the laser amplitude drift. To increase the high-frequency measurement range, a fringe-counting circuit could be added to the photodiode signal to allow for jumps in the operating point. It would also be possible to allow the nanopositioner to 'force' jumps in the operating point in order to extend the range. Although such improvements could enhance the performance, the additional complexity is not deemed commensurate. The proposed interferometer is most effective in its simplest form for the direct measurement of high-frequency vibrations with a peak-to-peak amplitude

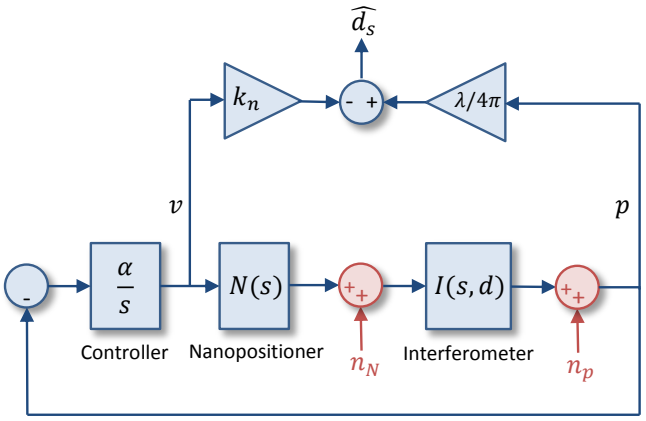

FIG. 7. The effect of nanopositioner noise (n_N) and photodiode noise (n_p) on the estimated displacement $\widehat{d_s}$.

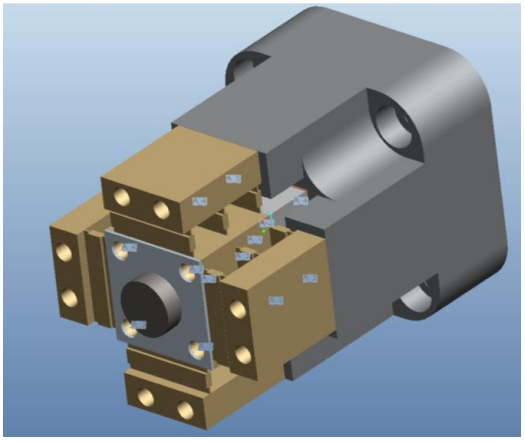

FIG. 8. A high-bandwidth piezoelectric mirror scanner.

of less than $\lambda/20$ (31 nm). This is ideal for measuring the frequency response of nanopositioners, electro-optical components, MEMs devices, ultrasonic devices, and sensors such as surface acoustic wave detectors.

VI. NOISE PERFORMANCE

Interferometers are sensitive to a number of random and systematic variations including laser wavelength drift, laser power noise, distortion of the optical medium, mechanical vibration, and photodiode noise[3]. These noise sources can be reduced or eliminated by a variety of techniques such as laser stabilization, higher laser power, and multi-beam compensation for the optical medium[3].

The entry points of noise into the proposed interferometer are illustrated in Figure 7. The two signals of interest are the nanopositioner noise n_N and the photodiode noise n_p. The nanopositioner noise is the random motion of the of nanopositioner. Since this appears at the same location as d_s, except for an opposite sign, the results in equation 14, can be employed directly. That is, the estimated displacement $\widehat{d_s}$ due to the nanopositioner noise is

$$\widehat{d_s} = -n_N. \tag{15}$$

This is significant since the noise spectrum of the nanpositioner appears directly at the estimated displacement. To minimize this source of noise, an open-loop nanopositioner can be used in applications where the low-frequency linearity is not important, for example, when measuring high-frequency vibration. The noise bandwidth can also be limited by filtering the voltage noise applied to the piezo, for example, with a series resistor or inductor.

The additive photodiode noise n_p can be used to model the photodiode electrical noise and other sources such as the laser shot, power, and phase noise. The cumulative power spectral density can be measured experimentally by fixing the reference and target mirrors. Since the interferogram is assumed to have a range of [-1,1], the spectrum should be measured after scaling has been performed, or it should be appropriately scaled after measurement. That is, the additive noise at the estimated displacement is

$$\widehat{d_s} = -n_p \frac{\lambda}{4\pi}. \tag{16}$$

The total power spectral density of the noise in the estimated displacement can be found by summing the power spectral densities,

$$S_{\widehat{d_s}}(f) = S_{n_N}(f) + \frac{\lambda^2}{16\pi^2} S_{n_p}(f). \tag{17}$$

Alternatively, the power spectral density of $\widehat{d_s}$ can be measured directly by fixing the target mirror and enabling the feedback loop. However, this approach will not reveal the relative magnitudes of the nanopositioner and photodiode noises.

VII. EXPERIMENTAL RESULTS

This section characterizes the performance of the proposed interferometer then demonstrates its use by measuring the frequency response of a dual-stage mirror scanner. The mirror scanner under investigation is illustrated in Figure 8. This device contains two stack actuators, one that provides slow (10 kHz) motion up to 10 μm and another that provides fast (100 kHz) motion up to 922 nm. This device was designed by Dr. Sachin Wadikhaye from the University of Newcastle. The experimental setup is pictured in Figure 4 and described in Section II.

A. Performance

To observe the time-domain resolution of the proposed interferometer, a reference displacement was created by

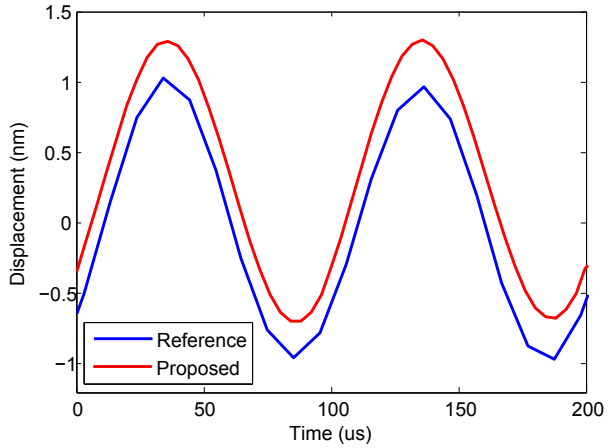

FIG. 9. A comparison between the proposed interferometer and a commercially available fibre-probe Fabry-Perot interferometer. The displacement of the sensing mirror is a 10 kHz sinusoid with an amplitude of approximately 1 nm. A 0.3-nm offset is added to the red waveform for clarity.

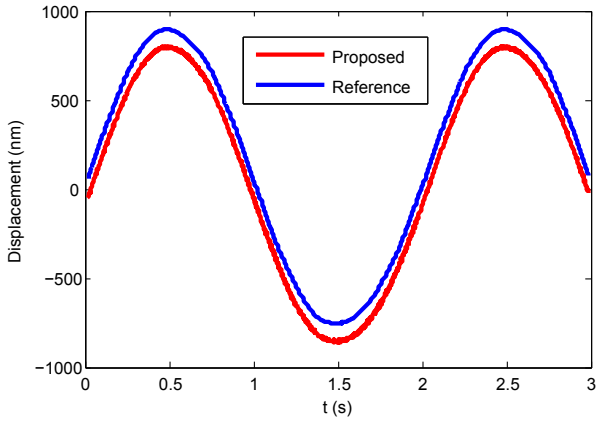

FIG. 10. A comparison between the proposed and commercial interferometers with a 1.7 μm displacement range. The signals are offset by 100 nm for clarity. The standard-deviation of the difference is 4.5 nm which indicates a close correlation.

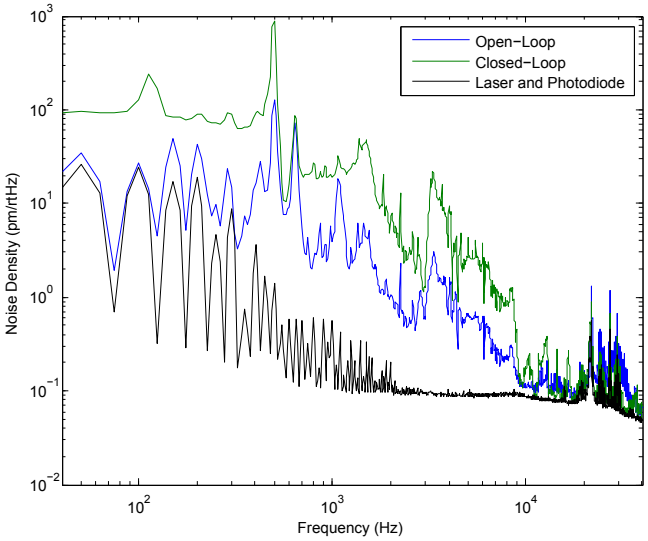

FIG. 11. Noise spectral density (in pm/$\sqrt{\text{Hz}}$) of the proposed interferometer with an open-loop and closed-loop nanopositioner.

driving the fast-stage actuator of the mirror scanner shown in Figure 8. The actuator is a Noliac NAC2025 piezoelectric plate (200V, 5x5x2 mm) which is mounted directly under the mirror. This arrangement develops a full-scale displacement of 922 nm from a 200-V drive signal. A 2-nm displacement was produced by applying a 0.5-V (p-p), 10-kHz sinusoidal voltage. This displacement was measured by the proposed interferometer and a commercially available fibre-probe Fabry-Perot interferometer. In order to compare the intrinsic resolution of both instruments, low-frequency noises due to building vibration, acoustics, and air-currents were removed by a fourth-order filter with a pass-band from 5 kHz to 20 kHz. The resulting signals are plotted in Figure 9. Both instruments can be observed to accurately resolve the 2-nm displacement. Note that the maximum sampling rate of the reference interferometer was 100 kHz (limited by USB interface) which results in obvious discretization. A benefit of the proposed interferometer is that the displacement signal chain is entirely analog which can be sampled at any rate or observed directly without digital hardware which is particularly useful when investigating high-bandwidth devices such as crystal resonators or surface acoustic wave sensors. In this experiment the displacement signal was recorded at 250 kHz by an oscillscope.

The proposed interferometer is also compared to the commercial interferometer with a slow displacement signal of 1.7 μm in Figure 10. With this range and frequency, the displacement signal is primarily derived from the control signal from the feedback loop.

The noise behavior of the interferometer was described in Section VI. In addition to the usual sources of noise due to air currents, photodiode noise, and laser noise, the proposed design is also sensitive to noise generated by the nanopositioner. To measure the experimental noise spectral density, the target mirror was fixed and the spectrum was recording with a Data Physics Quattro Spectrum Analyzer. The noise spectrum in Figure 11 considers two cases, one where the nanopositioner is operated in closed-loop, and another where it is operated in open-loop. The noise density due to the the laser and photodiode is also plotted in black, which is the minimum achievable noise density.

In the closed-loop results, the low frequency noise is approximately 100 pm/$\sqrt{\text{Hz}}$, which is the closed-loop positioning noise of the nanopositioner. At frequencies above the mechanical bandwidth of the nanopositioner (2 kHz), the noise reduces to the background noise of the laser and photodiode, which has a minimum noise density of approximately 0.1 pm/$\sqrt{\text{Hz}}$. The peaks between 20 and

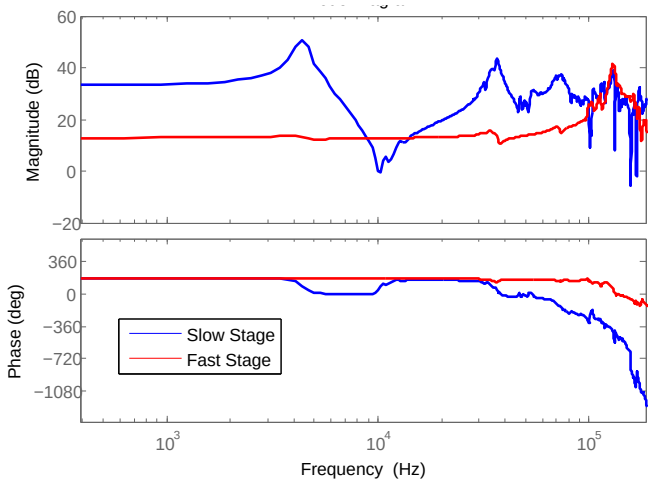

FIG. 12. Frequency response of the fast and slow stage of the mirror scanner (in pm/V).

40 kHz are due to the laser power supply ripple. The background noise limit of 0.1 pm/$\sqrt{\text{Hz}}$ is due to a combination of photodiode noise and stochastic laser noise.

To improve the low frequency noise, the nanopositioner was trialed in open-loop. This eliminates noise from the capacitive sensors and leaves only the voltage amplifier and mechanical noise. As shown in Figure 11, the open-loop nanopositioner significantly improves noise performance below 10 kHz. However, the penalty is reduced linearity when measuring large, low-frequency displacements. The use of an open-loop nanopositioner is recommended when the low-frequency linearity is inconsequential, for example, when measuring high-frequency displacements.

B. Demonstration

To measure the fast and slow stage frequency response, each actuator was driven by a 1-V RMS random signal using a PD200 voltage amplifier. The resulting frequency response measured with an HP spectrum analyzer is plotted in Figure 12. The first resonance frequency of slow stage is observed to be 4.4 kHz while the fast stage resonance frequency is 129 kHz. The second mode of the slow-stage is also significant in profile and occurs at 36 kHz. Due to the wide-bandwidth of the interferometer, there is no measurement phase-lag which can occur with capacitive and inductive sensors. This allows a precise measurement of the frequency response.

VIII. CONCLUSIONS

An interferometer is proposed with closed-loop control of the reference mirror. By locking the interferometer phase to the most sensitive point, high-frequency movements can be detected directly from the photodiode signal and low-frequency movements can be detected from the control signal. These signals are complementary and and be summed to find the total displacement of the sensing mirror.

The proposed interferometer is optically simple, does not require polarization or modulation to detect the direction of motion, does not require fringe-counting or interpolation electronics, and has a bandwidth equal to that of the photodiode. The low-frequency range of the interferometer is equal to the travel range of the reference mirror stage, while the high-frequency range is limited by the small angle approximation at the operating point which is most accurate when the peak-to-peak amplitude is less than $\lambda/20$ (31 nm), which can be extended to $\lambda/4$ by inverting the sinusoidal non-linearity. However, the uncompensated measurement range is ideal for measuring the frequency response of nanopositioners, electro-optical components, MEMs devices, ultrasonic devices, and sensors such as surface acoustic wave detectors.

ACKNOWLEDGEMENTS

This work was supported in part by the Australian Research Council Discovery Project DP120100487 and the Future Fellowship FT130100543.

[1] A. J. Fleming, Sensors and Actuators A: Physical **190**, 106 (2013).
[2] A. J. Fleming, Mechatronics **24**, 605 (2014).
[3] R. Loughridge and D. Y. Abramovitch, in *Proc. American Control Conference* (Washington DC, 2013) pp. 3692–3709.
[4] P. Hariharan, *Basics of interferometry, second edition* (Academic Press, 2007).
[5] H. Butler, IEEE Control Systems **31**, 28 (2011).
[6] S. Mishra, J. Coaplen, and M. Tomizuka, IEEE Control Systems **27**, 20 (2007).
[7] R. Merry, M. Uyanik, R. van de Molengraft, R. Koops, M. van Veghel, and M. Steinbuch, Asian Journal of Control **11**, 130 (2009).
[8] J. N. Dukes and G. B. Gordon, Hewlett-Packard Journal **21**, 2 (1970).
[9] G. E. Sommargren, in *Proc. Precision Engineering Conference* (Dallas, Texas, 1986).
[10] K. Karrai and P. Braun, in *Proc. Actuator* (Bremen, Germany, 2010) pp. 285–288.
[11] H. A. Deferrari, R. A. Darby, and F. A. Andrews, The Journal of the Acoustical Society of America **42**, 982 (1967).
[12] R. A. Kline, R. E. Green, and C. H. Palmer, The Journal of the Acoustical Society of America **64**, 1633 (1978).
[13] P. Cielo, F. Nadeau, and M. Lamontagne, Ultrasonics **23**, 55 (1985).
[14] Y. K. Yong, A. J. Fleming, and S. O. R. Moheimani, IEEE/ASME Transactions on Mechatronics **18**, 1113 (2013).
[15] K. K. Leang and A. J. Fleming, Asian Journal of Control **11**, 144 (2009).
[16] M. Fairbairn, S. O. R. Moheimani, and A. J. Fleming, IEEE/ASME Journal of Microelectromechanical Systems **20**, 1372 (2011).